Adaptive space and time numerical simulation of reaction-diffusion models for intracellular calcium dynamics

Ch. Nagaiah[1*], S. Rüdiger[2†], G. Warnecke[3‡], M. Falcke[4§]

[1] Institute of Mathematics and Scientific Computing, University of Graz, Austria

[2] Institute for Physics, Humboldt University, Berlin, Germany

[3] Institute of Analysis and Numerics, Otto-von-Guericke University, Magdeburg, Germany

[4] Max Delbrück Center for Molecular Medicine, Berlin, Germany

November 16, 2010

Abstract

Adaptivity in space and time for the numerical simulation of stochastic and deterministic equations for intracellular calcium dynamics is presented. The modeling of diffusion, reaction and membrane transport of calcium ions in cells leads to a system of reaction-diffusion equations. We describe the modulation of cytosolic and ER calcium concentrations close to the membrane of the cell organelle.

A conforming piecewise linear finite element method is used for the spatial discretization while linearly implicit methods, Rosenbrock type methods, are used for the time integration. We adopt a hybrid algorithm to solve the stochastic part. The space grid is adjusted to the strong localization of the calcium release following stochastic channel transitions. By automatically adapting the spatial meshes and time steps to the proper scales during the transition of channel states, the method accurately resolves the evolution of intracellular calcium concentrations as well as buffer concentrations. This article emphasizes the adaptive and efficient hybrid numerical simulations in two space dimensions. The presented work establishes the basis for future simulations in a realistic 3D geometry.

*nagaiah.chamakuri@uni-graz.at, Tel: +43 316 3805063, Fax: +43 316 3809815

†sten.ruediger@gmail.com

‡warnecke@ovgu.de

§falcke@hmi.de

1 Introduction

Calcium signalling is an important part of cellular information processing. The Ca^{2+} signal employed by a variety of processes is a transient increase of the concentration in the cytosol [5, 6, 26]. Increase of $[Ca^{2+}]$ is due to entry through the cell membrane or to Ca^{2+} release from internal storage compartments, specifically the endoplasmic reticulum (ER) and the sarcoplasmatic reticulum. It leads to the formation of spatio-temporal signals in the form of waves of high Ca^{2+} concentration traveling across the cell [28, 20, 13] and global oscillations [4, 29].

The multiplicity of length and time scales poses a specific challenge for any numerical treatment of the problem. Physiologically, it is now well established that currents of calcium through an individual channel lead to very localized calcium spots of nanometer extension. On the other hand, the calcium is rapidly transported over distances of several micrometers. Since calcium signals are generated by local feedback as well as coupling to distant channels by transport over a μm scale, we need an efficient and accurate numerical modeling of processes on both scales. We therefore choose a finite element method with local grid adaptivity for the space discretization and linearly implicit Runge-Kutta methods for the time discretization. Moreover, to solve the deterministic and stochastic simulations we used a hybrid algorithm. Here, we will discuss the following important factors in the numerical solution of the problem: space and time discretization, adapting the spatial meshes and automatic time steps to the proper scales according to channel transitions, the hybrid algorithm which couples the solving of deterministic and stochastic problems.

We will outline some of the problems which are encountered in the numerical simulations. At first, due to the multiple length scales of channels and clusters in the membrane, suitable numerical methods are mandatory. In this work we have chosen the finite element method for solving this problem. To capture the original structure of the cell, adaptive grid refinement is necessary to provide efficient and fast numerical solutions. Also adaptive space and time discretization methods are efficient during the intermediate time steps for this type of complex problems. The release of calcium through channel opening or closing occurs on the order of microseconds. These small time scales cannot be ignored, therefore an efficient time stepping method to capture these fast changes are needed. For this purpose the linearly implicit Runge-Kutta methods, which are very suitable for solving stiff ordinary differential equations, are used. The opening of channels occurs in the order of microseconds and when all channels are closed then the time step size is nearly in order of milliseconds, see [25]. For handling such fast changing step sizes an automatic time step procedure is suitable. To control the spatial discretization error, a-posteriori error estimators are computed to steer the mesh improvement by refinement and coarsening in each time step during the primal and dual solves in optimization algorithm. Various other forms of adaptive mesh refinement techniques were applied successfully for excitable media by varying the spatial or temporal resolution or both [9, 22, 34].

By locally refining the regions in a grid where the solution data have large errors, an adaptive mesh refinement algorithm can greatly reduce the size of grid points and hence the number of unknowns. A both space and time adaptive strategy will further

improve the simulation efficiency. The space and time adaptivity for the deterministic simulation of calcium dynamics is well presented in Nagaiah et.al [24] where the coupling of stochastic channel transition was not considered. The spatial grid adaptivity plays important role in the hybrid numerical simulations which shows a good improvement over the CPU time. The main motivation of the current article is that to present efficient and accurate numerical simulations based on the space and time adaptivity for the hybrid stochastic and deterministic simulations of calcium dynamics.

The high and fast concentration changes upon opening and closing of channels have a strong impact on the stochastic dynamics of channel binding and unbinding. The stochastic solver is based on the Gillespie method, but the usual Gillespie method solves stochastic processes where the propensities are constant during the subsequent transitions. However, the concentration and propensities are changes based on the channel opening and closing. For this purpose we have adopted a hybrid algorithm which couples the deterministic and stochastic equations, see Alfonsi et al. [2]. Two different types of time stepping methods are considered for solving the deterministic and stochastic processes. One is a linearly implicit Runge-Kutta method to solve the deterministic equations and the other is the Gillespie method to solve the stochastic equations. In both parts, deterministic and stochastic, we use the adaptive time scales to get fast and efficient numerical results.

Briefly, the adaptivity of the spatial grid is controlled by the error estimator by Zienkiewicz and Zhu [37], which is based on the average of local gradients of the solution. The classical embedding technique for ordinary differential equation integrators is employed to estimate the error in time. An automatic step size selection procedure ensures that the step size is as large as possible to guarantee the desired precision. We find that the PI-controller proposed by Gustafsson, Lundh and Söderlind [16] works very well for this problem. Our numerical realization is based on the public domain software package DUNE [3].

The paper is organized as follows: In the second section we present the model which comprises calcium-buffer binding, diffusion and transport through the ER membrane. We will then introduce our method and strategies for grid adaptation, finite-element discretization and time-stepping. Section 5 presents different simulation of test cases. The final section gives a short discussion of our work.

2 Deterministic equations

In this section we present the mathematical model equations in 2D which describe the evolution of calcium concentrations during the channel transitions, see for more details Falcke [12]. The model consists of equations for the following deterministic quantities: calcium concentration in the cytosol and the ER as well as concentrations of several buffers in the cytosol. As a simplification we do not consider the full three dimensional cytosolic and ER space but instead consider thin sheets below and above an idealized planar ER membrane. All concentrations are therefore two dimensional in space.

The evolution of concentrations will be determined by diffusion, transport of calcium

through the ER membrane, and the binding and unbinding of buffer molecules to calcium

$$\begin{aligned}
\frac{\partial c}{\partial t} &= D_c \Delta c + (P_l + P_c(r,t))(E-c) - P_p \frac{c^2}{K_d^2 + c^2}\,, \\
&\quad -(k_{b,s}^+(B_s - b_s)c - k_{b,s}^- b_s) - (k_{b,m}^+(B_m - b_m)c - k_{b,m}^- b_m)\,, \qquad (1)\\
\frac{\partial E}{\partial t} &= D_E \Delta E + \gamma \left[(P_l + P_c(r,t))(E-c) - P_p \frac{c^2}{K_d^2 + c^2} \right], \qquad (2)\\
\frac{\partial b_m}{\partial t} &= D_{b,m} \nabla^2 b_m + k_{b,m}^+(B_m - b_m)c - k_{b,m}^- b_m\,, \qquad (3)\\
\frac{\partial b_s}{\partial t} &= D_{b,s} \nabla^2 b_s + k_{b,s}^+(B_s - b_s)c - k_{b,s}^- b_s\,. \qquad (4)
\end{aligned}$$

Here c is the concentration of Ca^{2+} in the cytosol, E is the concentration in the ER. The transport through the ER membrane comprises three contributions. Calcium is moved from the ER into the cytosol through a leak current $P_l(E-c)$ and the channels: $P_c(r,t)(E-c)$. The latter term will be discussed in more detail below. Calcium is resequestered into the ER by pumps, the term proportional to P_p. The action of the pumps was found to be cooperative in calcium. The parameter K_d is the dissociation constant of the pumps.

The term proportional to P_c in Eqs. (1) and (2) models the current through an open channel. This current was found to depend on the cross-membrane concentration difference. For differences found in cell-physiological conditions, the current can be approximated by a linear dependence on $(E-c)$. The current is modeled as a source with constant density in a specified channel cluster region. The radius R_i of the cluster i with $N_{\mathrm{open},i}$ open channels is then given by

$$R_i = R_s \sqrt{N_{\mathrm{open},i}}\,.$$

Clusters are situated at fixed position $\mathbf{x}_i$. The flux term is given by

$$P_c(\mathbf{r},t) = \begin{cases} P_{ch} & \text{if } \|\mathbf{r} - \mathbf{x}_i\| < R_i \ \text{ for a cluster i,} \\ 0 & \text{otherwise.} \end{cases}$$

Note that in a model including the dynamics of channel gating the number of open channels is time-dependent. The corresponding value of P_{ch} can be found in Table 2. Altogether, the model equations are a system of reaction-diffusion equations. A well established theory exists for the system of reaction-diffusion equations in the literature [8, 27, 32, 33].

The concentrations of the mobile and stationary buffers bound to calcium in the cytosol are given by b_m and b_s, respectively. All buffers are assumed to be distributed homogeneously in the initial state. Total buffer concentrations in the cytosol are denoted by B_m or B_s, respectively. Experimentally, the total amounts of some buffers are known quite well, see [21, 36]. However, the amount of other buffers as for example the stationary buffer, comprising contributions from different calcium stores such as mitochondria, are not well known.

3 Stochastic channel dynamics

One of the principal reasons that modelers and computational scientists have become more interested in Ca^{2+} dynamics is that the concentration of Ca^{2+} shows highly complex spatio-temporal behavior. Many cell types respond to agonist stimulation with oscillations in the concentration of Ca^{2+} . The process causing random behavior in intracellular Ca^{2+} dynamics is the transition between the different states of the channel subunits and the channel. Channels open and close randomly. The opening and closing probability depends on the state of the channel subunits.

In this subsection, the stochastic model for the gating of subunits is explained. This model is based on the DeYoung-Keizer (DYK) model for the subunit dynamics, see [11]. Details of the modified DYK model which is used in our numerical calculations can be found in [30]. It is known that a subunit has binding sites for Ca^{2+} and IP_3 . Based on the results of Bezprozvanny et al. [7], DeYoung and Keizer [11] proposed a model for a single subunit. The model by DeYoung and Keizer was set up as a deterministic model and used later on as a stochastic scheme by Falcke et al. [12, 14]. The subunit has three binding sites: an activating and an inhibitory Ca^{2+} as well as an activating IP_3 binding sites.

In this work the stochastic solver is based on the Gillespie method [15]. The Gillespie algorithm uses random pairs (r_1, r_2) and the equations

$$a_0 \cdot \tau = \ln(1/r_1)\,, \sum_{j=1}^{i} a_j \leq a_0 \cdot r_2 < \sum_{j=1}^{i+1} a_j\,. \tag{5}$$

Using this random pair we can find the next event R_i and that it will occur after time τ.

The Gillespie method is based on the assumption that during successive stochastic events the propensities a_i do not change. Indeed, over those successive stochastic events, there must be a significant activity in all reaction channels. However, when linking the stochastic channel dynamics to the calcium dynamics, we expect the propensity a_i to change in time due to its dependence on the local calcium concentration c. This effect will be particularly strong for openings and closings of channels, since after such events the local calcium concentration c changes dramatically by orders of magnitude. So the propensities can change too rapidly over small time intervals.

To overcome those problems, a hybrid method is adopted which was introduced by Alfonsi et al. [2]. In their hybrid algorithm, the stochastic reaction equations are partitioned into deterministic and stochastic equations, to reduce the computational time and increase the efficiency. To adapt this hybrid algorithm to current problem, we used that the spatial-temporal equations are deterministic and the opening/closing of channels is considered as stochastic part. Here we will give a brief explanation of the hybrid method.

Within their setting the time τ to the next stochastic event is determined by solving

$$g_i(t+\tau|t) = \int_t^{t+\tau} a_i(c(t), s)\, ds = \xi\,, \tag{6}$$

with $\xi = \ln(1/r_1)$, where the sum of propensities a_0 may explicitly depend both on time and the local calcium concentration. The function $g_i(t+\tau|t)$ is non-decreasing for $t+\tau > t$,

since the propensities a_i are non-negative by definition. Note that the above equation simplifies to the equation determining τ in Eq. (5) in the case of constant a_0. To determine the time of next reaction τ, condition Eq. (6) is conveniently rewritten in differential form by introducing a variable $g(t)$ and solving

$$\dot{g}(s) = a_0(c, s) \tag{7}$$

with initial condition $g(0) = 0$, along with the deterministic equations for c and buffers. To calculate the propensities we follow the dynamics of the DYK model.

We would like to give the brief outline of the algorithm here. A special feature of the calcium system is that not all stochastic events change the open/closed state of a channel. A channel transition has a major impact on the local calcium concentration c, while non-channel transitions do not change the local calcium concentration. During the computation of the deterministic part of the calcium dynamics the stochastic events are traced via Eq. (6) respectively Eq. (7). During the simulation the stochastic system is updated for every stochastic time step dt. The time step dt is determined using the first random number generation, see Eq. (5), and by fulfilling the requirement $a_0 dt \leq 1$, where a_0 is the sum of the propensities. Using the second random number the reaction event R_i is determined, see Eq. (5). In this way we can determine the next reaction event R_i and it will occur after the time τ. If a non-channel transition occurs, the stochastic event is performed. The stochastic channel dynamics is updated correspondingly, while there is no influence on the calcium concentration. On the other hand, if a channel transition takes place, both the channel and the calcium dynamics do change. This typically requires a readjustment of the deterministic time step which will be explained in later sections. The algorithmic realization of our hybrid approach is given in [30, 23] and the extension of the algorithm by using the spatial grid adaptivity is given at the end of section 4. .

4 Numerical method

4.1 Spatial discretization using finite elements

The state variables $c(\underline{x}, t)$, $E(\underline{x}, t)$, $b_m(\underline{x}, t)$ and $b_s(\underline{x}, t)$ are functions of space and time on in $\Omega \times [0, T]$ where the domain $\Omega \subseteq \mathbb{R}^2$ is a convex polygonal subset. In this section we describe the finite element method for solving the coupled reaction-diffusion system (1-4). We will first consider a so-called *semi-discrete* analogue of the full system where we have discretized in space using the continuous piecewise linear finite elements. The formulation and subsequent discretization of such an integral form requires the definition of some function spaces and associated norms. Consider a spatial domain $\Omega \subset \mathbb{R}^2$ with piecewise smooth boundary Γ. We shall denote by $L^2(\Omega)$ the space of functions that are square-integrable over the domain Ω, see Adams [1] for other notations.

4.2 Semi discretization in space

Consider the parabolic prototype problem

$$\begin{aligned} \tfrac{\partial u(\mathbf{x},t)}{\partial t} - \nabla \cdot (D \nabla u(\mathbf{x},t)) + s(u,\mathbf{x},t) = 0 \quad &\text{in} \quad \Omega \times (0,T]\,, \\ u(\mathbf{x},t) = u_0(\mathbf{x}) \quad &\text{on} \quad \Omega \times t = 0\,, \\ \mathbf{n} \cdot \nabla u(\mathbf{x},t) = 0 \quad &\text{on} \quad \partial\Omega \times [0,T]\,, \end{aligned} \tag{8}$$

where $u(\mathbf{x},t)$ is unknown, $D \in \mathbb{R}^{2\times 2}$ is assumed to be diagonal with positive coefficients and $s(u,\mathbf{x},t)$ is the reaction function. The discretization process using the finite element method is based on a reformulation of the given differential equation in the more general, *variational formulation*. Let $V = H^1(\Omega)$ and V_h be a finite dimensional subspace of V with basis $\{w_1,\ldots,w_N\}$. Specifically we take continuous functions that are piecewise linear on a quasi-uniform triangulation of Ω with mesh size h. Replacing the space V by the finite dimensional subspace V_h we get the following *semi discretization in space* find $u_h \in V_h$ s.t.

$$\begin{aligned} \langle \tfrac{\partial u_h}{\partial t}, v_h \rangle + \langle D\nabla u_h, \nabla v_h \rangle + \langle s(u_h,\mathbf{x},t), v_h \rangle = 0 \quad &\text{for all} \quad v_h \in V_h\,, \\ u_h(\mathbf{x},t) = u_{0,h}(\mathbf{x}) \quad &\text{on} \quad \Omega \times t = 0\,. \end{aligned} \tag{9}$$

In particular, since V_h is a linear space of dimension N with basis $\{w_i\}_{i=1}^N$, taking $v_h = w_j$, we get a system of ordinary differential equations in the form

$$\mathcal{M}\dot{u} = -\mathcal{A}u - \mathcal{S}\,, \tag{10}$$

where $\mathcal{M}$ is the mass matrix, $\mathcal{A}$ is the stiffness matrix and $\mathcal{S}$ is a vector depending on the reaction term. The matrices are defined as follows

$$\begin{aligned} &\mathcal{M} = \langle w_i, w_j \rangle\,, && \mathcal{A} = \langle D\nabla w_i, \nabla w_j \rangle\,, \\ &\mathcal{S} = \langle s(\textstyle\sum_{i=1}^N u_i(t) w_i(x)), w_j \rangle\,. \end{aligned}$$

In our numerical simulations we considered the free calcium concentration in the cytosol, the free calcium concentration in the ER, and the stationary and mobile buffers in the cytosol. We can apply the analogous spatial discretization to Eqs. (1-4). Then we get the ordinary differential equation system as follows

$$\mathbf{M}\dot{\mathbf{u}} = -\mathbf{A}\mathbf{u} - \mathbf{S}\,,$$

where the block diagonal matrices $\mathbf{M} = \mathrm{diag}(\mathcal{M},\mathcal{M},\mathcal{M},\mathcal{M})$, $\mathbf{A} = \mathrm{diag}(\mathcal{A},\mathcal{A},\mathcal{A},\mathcal{A})$ and $\mathbf{S}$ is a $4N \times 1$ vector depending on reaction terms.

4.3 Temporal time-stepping of continuous equations

The discretization in time of Eq. (10) can be accomplished in several possible ways. We have mainly concentrated on implicit methods for solving these equations. For solving problem we used higher order linearly implicit methods of Rosenbrock type. These methods offer several advantages. They completely avoid the solution of nonlinear equations, which

means that no Newton iteration has to be controlled. More detailed expositions of these methods can be found in [17, 18]. Moreover, for computation of adaptive time step a simple embedding technique can be utilized to estimate the error part arising from the time discretization. An automatic step size selection procedure ensures that the step size is as large as possible while guaranteeing the desired precision.

We considered the ODE problem

$$\mathbf{M}\frac{\partial \mathbf{u}}{\partial t} = \mathbf{F}(t, \mathbf{u}), \qquad \mathbf{u}(t^0) = \mathbf{u^0}. \tag{11}$$

To start with, we partition the time $[0, T]$ into discrete steps $0 = t^0, t^1, \ldots, t^n = T$, that are not necessarily equidistant. The notation for time step is $\tau^i = t^{i+1} - t^i$ and $\mathbf{u}^i$ to be the numerical solution at time t^i. For computation an s-stage *Rosenbrock* method of order p with embedding of order $\hat{p} \neq p$ has the form

$$\begin{aligned}
(\frac{1}{\tau^i \gamma}\mathbf{M} - \mathbf{J})\mathbf{k}_j &= \mathbf{F}\left(t^i + \tau^i \alpha_j, \mathbf{u}^i + \sum_{l=1}^{j-1} a_{jl}\mathbf{k}_l\right) - \mathbf{M}\sum_{l=1}^{j-1}\frac{c_{lj}}{\tau^i}\mathbf{k}_l\,, \quad j = 1, \ldots, s\,, & (12)\\
\mathbf{u}^{i+1} &= \mathbf{u}^i + \sum_{l=1}^{s} m_l \mathbf{k}_l\,, & (13)\\
\hat{\mathbf{u}}^{i+1} &= \mathbf{u}^i + \sum_{l=1}^{s} \hat{m}_l \mathbf{k}_l\,. & (14)
\end{aligned}$$

Here $\mathbf{J} = \partial\mathbf{F}/\partial\mathbf{u}$ is the Jacobian matrix. For the construction of the Jacobian matrix we used exact derivatives of the vector $\mathbf{F}(t, \mathbf{u})$. The method coefficients $\gamma, \alpha_j, a_{jl}, c_{jl}, m_l$, and $\hat{m}_l$ are chosen such a way that certain order conditions are fulfilled to obtain a sufficient consistency order and good stability properties. Replacing the coefficients in Eq. (13) by different coefficients $\hat{m}_l$ a second solution $\hat{\mathbf{u}}^{i+1}$ of lower order $\hat{p}$, where $\hat{p} < p$, can be constructed [17, 18] .

Usually, for the complex dynamical behavior problems, for instance the current problem under consideration, the fixed time steps are not adequate to do longer time horizon which require a huge number of small time steps. Thus, time step adaptation is an important and should be efficient in order to control the temporal error. After the i-th integration step the value $\epsilon^{i+1} = \|\mathbf{u}^{i+1} - \hat{\mathbf{u}}^{i+1}\|_{L^2}$ is taken as an estimator of the local temporal error. A new time step τ_{new}, see Gustafsson et al. [16], is computed by

$$\bar{\tau} := \beta\frac{\tau^i}{\tau^{i-1}}\left(\frac{TOL_t}{\epsilon^{i+1}}\right)^{\frac{p_2}{p}}\left(\frac{\epsilon^i}{\epsilon^{i+1}}\right)^{\frac{p_1}{p}}\tau^i, \quad \tau_{\text{new}} = \begin{cases} \beta_{\max}\tau^i, & \bar{\tau} > \beta_{\max}\tau^i,\\ \beta_{\min}\tau^i, & \bar{\tau} < \beta_{\min}\tau^i,\\ \bar{\tau}, & \text{otherwise.}\end{cases} \tag{15}$$

The parameter $\beta > 0$ is safety factor. The factors $\beta_{\min}$ and $\beta_{\max}$ restrict time step jumps. In our computations we have chosen the parameters $p_1 = 1$ and $p_2 = 1$. If $\epsilon < TOL_t$, where TOL_t is a desired tolerance prescribed by the user, we proceed to the next time

step, otherwise the time step has to be shortened according to Eq. (15) and a new try is performed.

The simulations are performed using the ROS2 method [10] which is a 2nd order method with 2(1) internal stages, and ROS3P [19], W-method [31] as well as ROWDA [18] which are 3(2) order methods with 3 internal stages. Finally, after time discretization, we get a system of algebraic equations in each internal stage. For solving the algebraic system in each stage we used the BiCGSTAB method with ILU preconditioning.

4.4 Spatial grid adaptivity

The adaptive mesh refinement(AMR) algorithm try to automatically refine or coarsen the mesh to achieve a solution having a specified accuracy in an optimal fashion and it uses a hierarchy of properly nested levels. For this problem we considered the AMR technique based on the Z^2 error indicator of Zienkiewicz and Zhu [37] which is based on the averaging gradients of the solution. See also [35] for a more detailed description of error estimators. The full spatial and temporal discretization leads to an approximate solution u_h^t with $u_h^t(\cdot, t_i) \in V_h$ at the discrete time points t_i, $i = 0, \ldots, M$ where the time integration scheme is evaluated. Here we will recall the Z^2 error indicator.

We denote by W_h the space of all piecewise linear vector-fields and set $X_h := W_h \cap C(\Omega, \mathbb{R}^2)$. Denote u and u_h the unique solution of problems (8) and (9), respectively. Let $Gu_h \in X_h$ be the $\langle \cdot, \cdot \rangle_h$-projection of ∇u_h onto X_h. In this case $\|Gu_h - \nabla u_h\|_{L^2(T)}$ can be used as an error estimator, where Gu_h is an easily computable approximation of ∇u_h, see [35] for more details. It can be computed by a local averaging of $\nabla u_{h|T}(\mathrm{x}_i)$ as follows

$$Gu_h(\mathrm{x}_i) = \sum_{T \subset D_{x_i}} \frac{|T|}{|D_x|} \nabla u_{h|T}(\mathrm{x}_i)\,. \tag{16}$$

Here, D_{x_i} is the union of the triangles having x_i as a vertex and $|T|$ denotes the area of triangle T. Thus, Gu_h may be computed by a local averaging of ∇u_h. We finally set

$$\eta_{Z,T} := \|Gu_h - \nabla u_h\|_{L^2(T)}\,, \tag{17}$$

and

$$\eta_Z := \left\{ \sum_{T \in \mathcal{T}_h} \eta_{Z,T}^2 \right\}^{1/2}. \tag{18}$$

The Z^2 indicator $\eta_{Z,T}$ is an estimate for $\|\nabla u_h^t(\cdot, t_i) - \nabla u^t(\cdot, t_i)\|_{L^2(T)}$, see Verfürth [35]. Let $\lambda(T) \in \mathbb{N}_0$ be the refinement level of triangle $T \in \mathcal{T}$, $\lambda_{max} \in \mathbb{N}_0$ be a given maximum refinement level, and $\phi_1, \ldots, \phi_{\lambda_{max}}$ be given real numbers satisfying $0 \leq \phi_1 \ldots \leq \phi_{\lambda_{max}}$. We set $\phi_0 = 0$ and $\phi_{\lambda_{max}} = \infty$. With the choice of $\phi_1, \ldots, \phi_{\lambda_{max}}$ one controls the structure of the grid. If we set $\phi_1 = \ldots = \phi_{\lambda_{max}} = 0$ this leads to a uniform triangulation of level λ_{max}.

In our numerical computations, the fully coupled space-time adaptive algorithm is introduced as follows. Suppose that an initial coarse triangular grid is constructed using grid generator. To generate the initial coarse adaptive grid, we use a strongly localized function as initial solution in the vicinity of the cluster area for error estimator. To account for the exponential decay of calcium away from the source we generate a succession of localized functions with decreasing spatial extent. Then we refine the mesh until a minimum of 9 grid points lie in the area of each channel. A triangle T is marked for

1. refinement if $\eta_{Z,T} > \phi_{\lambda(T)}$ and $\lambda(T) < i \quad$ for $i = 0, \ldots, \lambda_{max}$,

2. coarsening if $\eta_{Z,T} < \frac{\phi_{\lambda(T)}}{100}$ and $\lambda(T) > i \quad$ for $i = 0, \ldots, \lambda_{max}$,

where $\eta_{Z,T}$ is calculated according to Eq. (17). At this level, the constructed mesh is assumed as a coarse mesh when simulation starts, denoted by L_0, and it will be the central part of the root level of the hierarchical system. It is fixed during the process of adaptive mesh refinement. Finer levels L_i for $i > 0$ are constructed recursively from the coarser levels L_{i-1}. In our numerical computations, the tolerance for spatial grid refinement is set $Tol_x = 10^{-3}$. The Z^2 error estimator is called for every 3 time intervals while solving the deterministic part and adapt the grid if the spatial error is greater than the given prescribed tolerance Tol_x. Thus, it adjusts the spatial grid by refining and coarsening, depending on the estimated spatial solution error of the elements. Accordingly, the new solution is updated based on the new grid construction via linear interpolation. After advancing the solution data to the new grids, the time discretization step has been applied and the new solution is computed. If the computed time error, based on a simple embedding technique, is less than the prescribed tolerance then step has to be proceeded further. If not, time step has to be shortened based on the time step controller and repeated the time step procedure again. In this way, both time step control and dynamic mesh refinement based on a posteriori error estimation can be simultaneously realized in our numerical experiments.

Here we present algorithmic aspects of hybrid stochastic and deterministic numerical simulations by utilizing the spatial grid adaptivity as follows where u represent the solution vector (c, E, b_m, b_s).

1. Initialization

   - Choose $u_{old} = u_0$ $X = X_0$, $g_{old} = 0$, $t_{old} = 0$, $\Delta t > 0$, and draw a uniform random number r_1 in [0,1] defining $\xi = \ln(1/r_1)$.

2. Deterministic step

   - Update the new solution u_{new} and g_{new} by utilizing the AMR technique which was explained in section 4.4.
   - If the tolerance for the temporal adaptation procedure is not met, reduce the step size Δt and go to 2 where the fine (refined) grid is considered for this step. Otherwise update the $t_{new} = t_{old} + \Delta t$ and set the new step size Δt according to the time stepping code prediction.

3. If $g_{new} < \xi$ (no stochastic event)

   - Set $u_{old} = u_{new}$, $g_{old} = g_{new}$, $t_{old} = t_{new}$, and go to 2.

4. If $g_{new} \geq \xi$ (some stochastic event in the time interval $[t_{old}, t_{new}]$)

   - Determine the event time $t_s \in [t_{old}, t_{new}]$ by (linear) interpolation, and compute the corresponding calcium concentration c_s at the event time t_s by (linear) interpolation.
   - Draw a uniform random number r_2 in $[0, 1]$ and determine the stochastic event R_i according to Eq. (5) based on c_s.

5. If the next event R_i is non-channel transition

   - Perform the stochastic event R_i to determine the new channel state X.
   - Set $g_{old} = 0$ and recompute g_{new} based on c_s, g_{old} and the remaining time $(t_{new} - t_s)$.
   - Draw a new uniform random number r_1 in $[0, 1]$ defining $\xi = \ln(1/r_1)$, and go to 3.

6. If the next event R_i is a channel transition

   - Perform the channel transition R_i to determine the new state X.
   - Set $g_{new} = 0$, and draw a new uniform random number r_1 in $[0, 1]$ defining $\xi = \ln(1/r_1)$.
   - Set $t_{new} = t_s$, and define new step size $\Delta t = \Delta t_{channel}$ (a sufficiently small number).
   - Set $u_{old} = u_s$, and go to 2.

5 Numerical results

In this section we describe numerical simulations that are performed on a squared geometry, $[0\,, 33000] \times [0\,, 33000]\ nm^2$, as computational domain with refinement by using triangular elements. This domain represents the ER membrane. In the following subsections we show the convergence of numerical solutions with different time stepping methods as well as adaptive grids. The parameters that have been used in the numerical simulation are shown in Table 2. The initial solution for concentrations and buffers is considered as constants over the computational domain.

All numerical computations were performed by using a Linux machine with 2 GB RAM, 2.33 GHz processor, gcc-4.1.0 compiler and the program package DUNE [3] which is a public domain and written in C++.

5.1 Results for deterministic opening and closing of channels

In this subsection we present the numerical tests based on the deterministic opening and closing of one channel in one cluster arrangement with a static grid and temporal adaptive grids. The initial coarse grid is shown in Figure 1(a) which is used in the case of adaptive grid refinement. The static (fine) grid is shown in Figure 1(b).

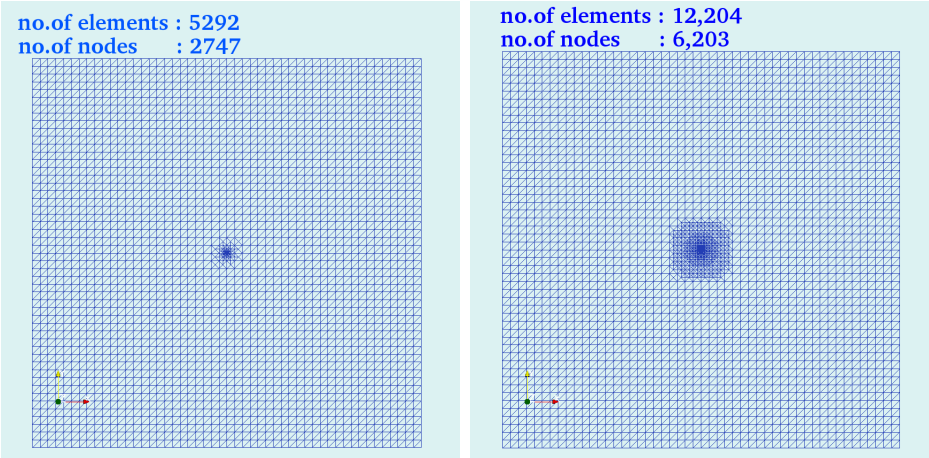

(a) (b)

Figure 1: Different grids considered for the simulation of arrangement of 1 cluster setup 1(a)) coarse grid which is considered as initial grid for adaptive grid refinement simulations, 1(b)) fixed grid for other simulations.

methods	accepted time steps	rejected time steps	total CPU time (hours)
ROS2	23446	63	38.78
ROS3p	9844	1151	30.83
ROWDA	5446	31	27.20
W-method	8794	366	27.37

Table 1: Comparison between different methods.

These results are presented for the opening and closing of one channel in one cluster arrangement for short period of times. The channel is opened at times $t = 0\ s$, $t = 1.0\ s$ and so on, whereas closing of the channel occurs at times $t = 0.7\ s, 1.7\ s, \ldots$ and so on. The numerical results are presented till time $t = 5\ s$ for different time stepping methods, like ROS2, ROS3p, ROWDA and W-methods. For these methods the accepted time steps, rejected time steps and total CPU time for the simulation is presented in Table 1. For the sake of examination of the convergence of solutions and the performance of several Rosenbrock methods we used the same tolerance $TOL_t = 10^{-5}$ for all methods which is a

small tolerance for the automatic time step selection procedure. Also, it is well known that each method shows a computational efficiency by properly adjusting the tolerance for time adaptivity. The maximum and average cytosolic calcium concentrations are presented for these methods in Figure 2. We can observe that for all integrators the maximum cytosolic calcium concentration lies on one curve except for the W-method. A closer look in the solution interval [7.0, 8.8] reveals that the W-method produces a slower propagation of excitation of calcium wave front compared to the other Rosenbrock solvers. The reason for this behavior might be a insufficient resolution in space or time for the W-method. The best performance with respect to accuracy and computing time is obtained by ROWDA method. Also, in a few other simulations, we experienced that ROWDA method works very well for smaller tolerances which is used in automatic time step selection, say $TOL_t = 10^{-4}$ to 10^{-3} , and saves a lot computational time to obtain the accurate solution. From Table 1, we can observe that ROWDA reaches the final time in 5,446 steps, Ros3p needs 9,844 steps, W-method 8,794 steps, and Ros2 even 23,446 steps. Due to the small tolerance and lower order of Ros2 method, it takes more accepted steps compare to other methods. In each accepted time step, for this method, the linear solver takes less number of iterations to converge the solution. We have experienced that if we increase the tolerance for time step control the Ros2 method also takes less accepted time steps and computational time is saved up to about 6%. Due to the 3 stages of the ROWDA method, it takes less accepted time steps and needs more linear solver iterations to converge the solution in comparison to Ros2 method.

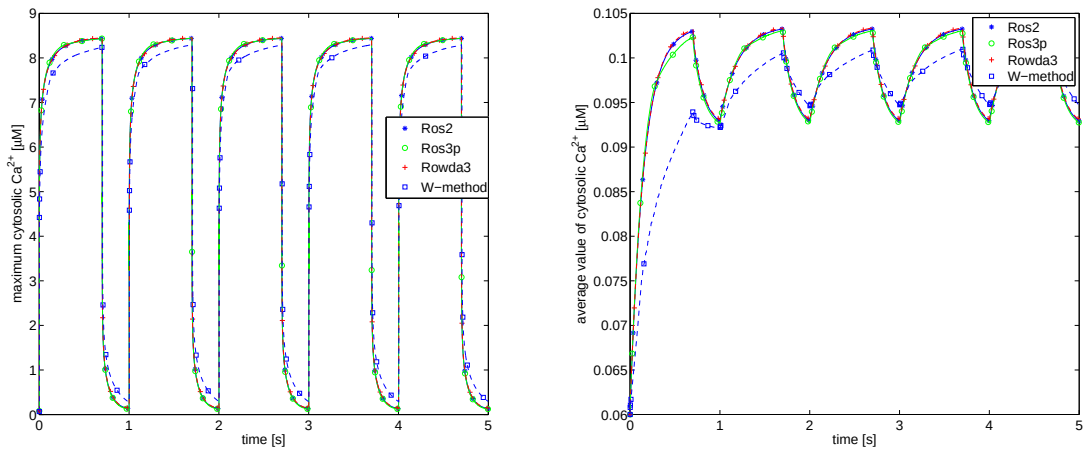

(a) (b)

Figure 2: The maximum and average cytosolic calcium concentration in 2(a) and 2(b) respectively for all time integrators.

For further numerical computations, we used the ROWDA method as a time integrator. Next, we examine the performance of different space resolution grids (different fine grid

levels) and the AMR grid and the numerical results are presented till time $t = 3\ s$. The difference between the solutions of maximum cytosolic calcium concentration for the fine grid levels 17, 18, 19, 20, and 21 which consists of 749, 837, 1,669, 2,061 and 3,225 grid points respectively within the area of one channel, and the AMR grid is presented in Figure 3(a). The zoom of this solution is shown in Figure 3(b). From these plots, it can be observed that the solution converges for finer meshes as well as for temporal adaptive grid. Also the average cytosolic calcium concentration and average ER calcium concentration are presented in Figure 3(c) and Figure 3(d) respectively. When a channel opens, the maximum cytosolic Ca^{2+} concentration raises rapidly and stays for a while. When an open channel closes the Ca^{2+} concentration falls immediately and recovers the stationary solution. These presented numerical results show that the temporal adaptive grid refinement solution is accurate as the fine grids during the intermediate time steps.

The corresponding number of elements, nodes and intermediate levels are shown in Figure 4. Here we can see that grid refinement strategy refines many elements after opening of a channel and this leads to more accurate solutions for this problem instead of considering the fixed grid. Refined elements are coarsened when all channels are closed. Also it proves that it saves more CPU time for the higher cluster set ups which we will present in later subsections. In our numerical implementation we have a flexibility to restrict the maximum number of elements and/or maximum number of refinement levels for grid refinement strategy, which is more useful to perform computations for higher cluster setups while considering the stochastic channel transition with moderate CPU time.

To give the comparison of CPU times for static grid and AMR grid, we considered the time interval for channel transition is 0.02s and total simulation time is 0.16s. Here the finest level of AMR mesh, during the intermediate time steps, is considered as static grid. In this case, the static grid takes 4300.57 seconds and AMR grid 3157.07 seconds of CPU time. It shows clearly that for one cluster setup the AMR method is faster. These results strive forward to apply AMR technique for more cluster setup considering the stochastic channel opening and closings.

5.2 Hybrid numerical results

In this subsection, the adaptive numerical solutions of calcium concentrations with stochastic channel transition are presented. To find a suitable time step is a very crucial task in these stochastic simulations to obtain a moderate overall computational time. In our numerical simulations deterministic and stochastic equations are coupled and require two different time steps. One time step for solving the deterministic equations, which is solved by using the linearly implicit Runge-Kutta method and the other for solving the stochastic part, where we use the Gillespie algorithm. Both are adaptive with regard to time stepping.

5.2.1 Numerical results with one cluster set up

In this subsection, the hybrid numerical results are shown based on the one cluster set up which consists of 20 channels. The simulation time is taken to be $t = 30\ s$ and results are

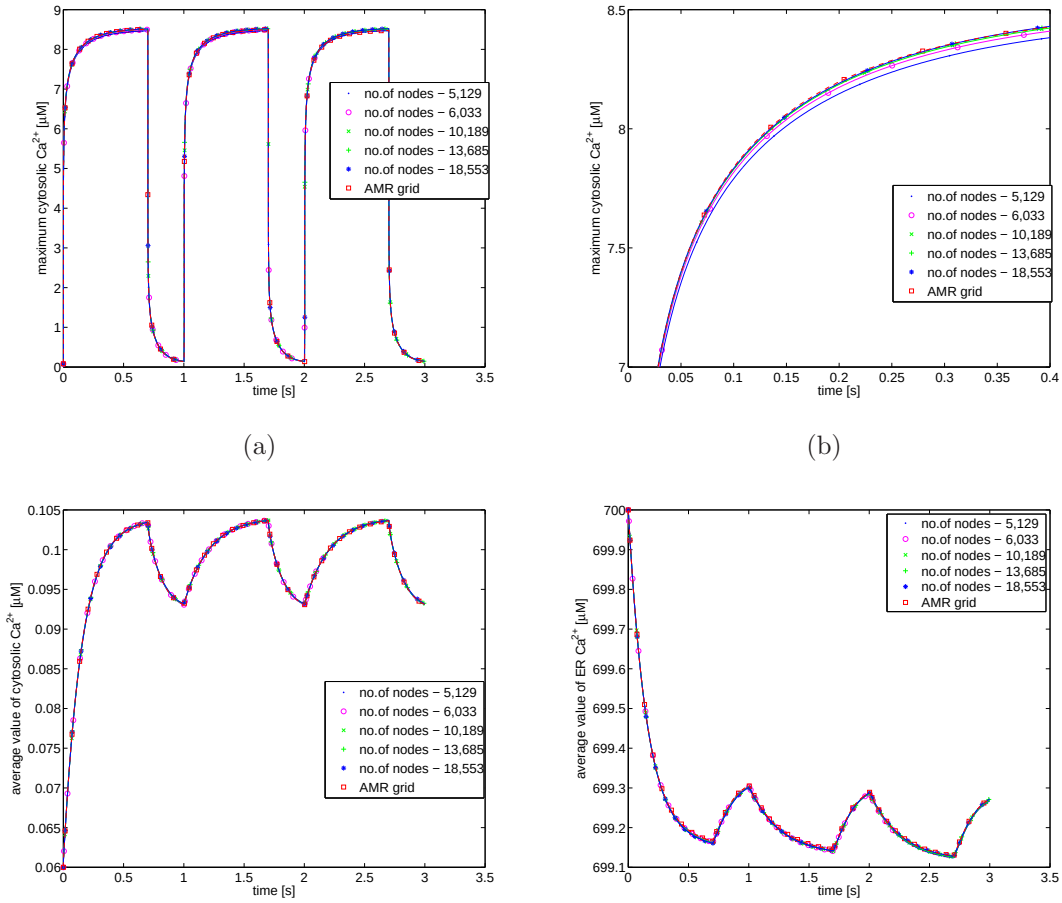

Figure 3: Comparison results over time for fine grids and temporal adaptive grids, maximum cytosolic calcium concentration and local zoom of this solution in 3(a)) and 3(b)) 3(c)) average value of cytosolic calcium concentration, 3(d)) average value of ER calcium concentration over the simulation time.

presented for a fine grid and adaptive grid. The concentration changes occur rapidly when a channel opens and closes. It stays constant when all channels are closed, as is shown in Figures 5(a) for maximum cytosolic concentration over time and maximum number of open channels over time in Figures 5(b). Figure 5(a) shows that the Ca^{2+} concentration is constant until approximately $t = 1\ s$ because no channel is opened during this time and after this time the Ca^{2+} concentration rapidly changes due to channel opening and closings. The corresponding maximum concentration over time and maximum number of open channels over time are given in Figures 5(c) and Figures 5(d) respectively for adaptive grids.

Typically, in these simulations the time step reduces to $10^{-8}\ s$ during the channel

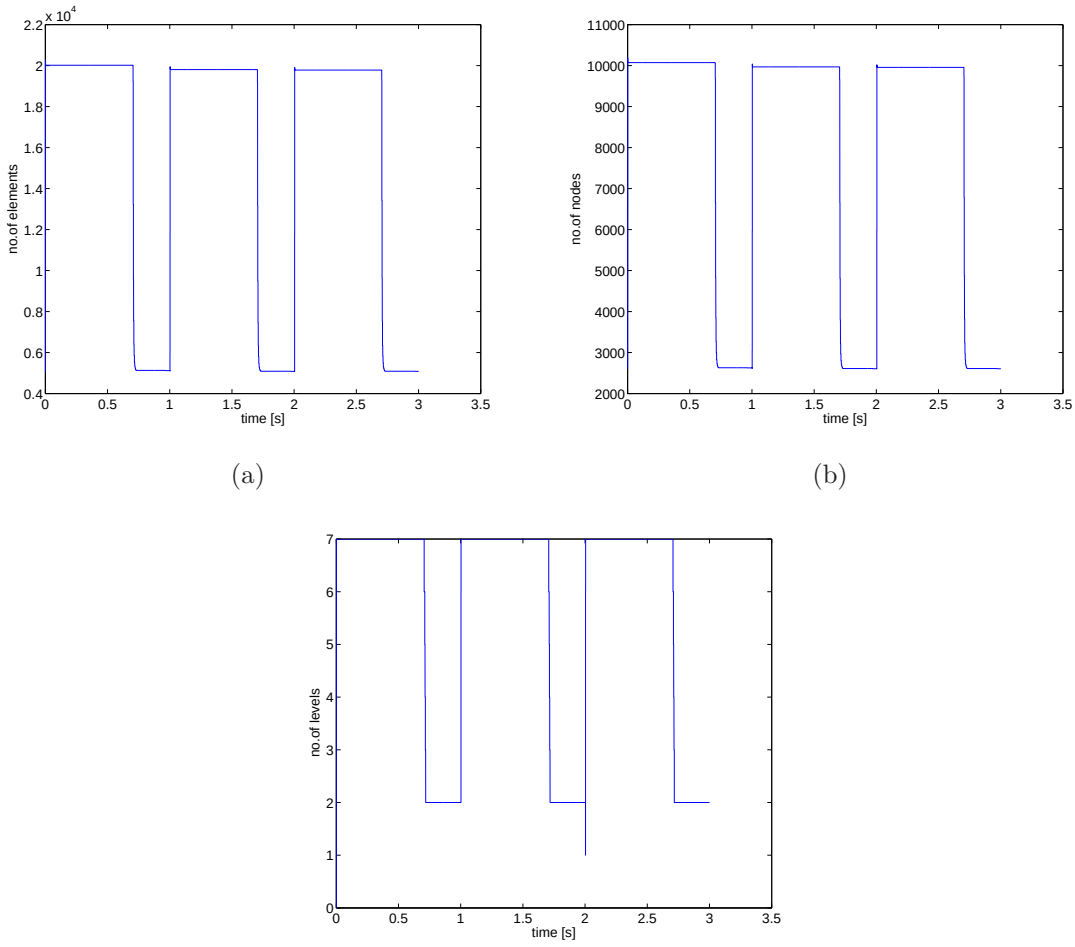

Figure 4: 4(a)) Number of refined elements, 4(b)) number of refined nodes and 4(c)) number of intermediate levels during the intermediate time steps for the adaptive grid refinement strategy over the simulation time.

opening and it returns to 10^{-2} s when all channels are closed. During this fast change the adaptive time step control plays an important role to maintain the accuracy of the solution. The corresponding average cytosolic and ER calcium concentrations, as well as the mobile and stationary buffer concentrations are plotted in Figure 6.

The evolution of the number of elements and number of points are shown in Figure 7 during the stochastic channel transition. The tolerances for the time $TOL_t = 10^{-4}$ and space $TOL_x = 10^{-3}$ are fixed. The behavior of local error control works as optimal as during the stochastic channel transition.

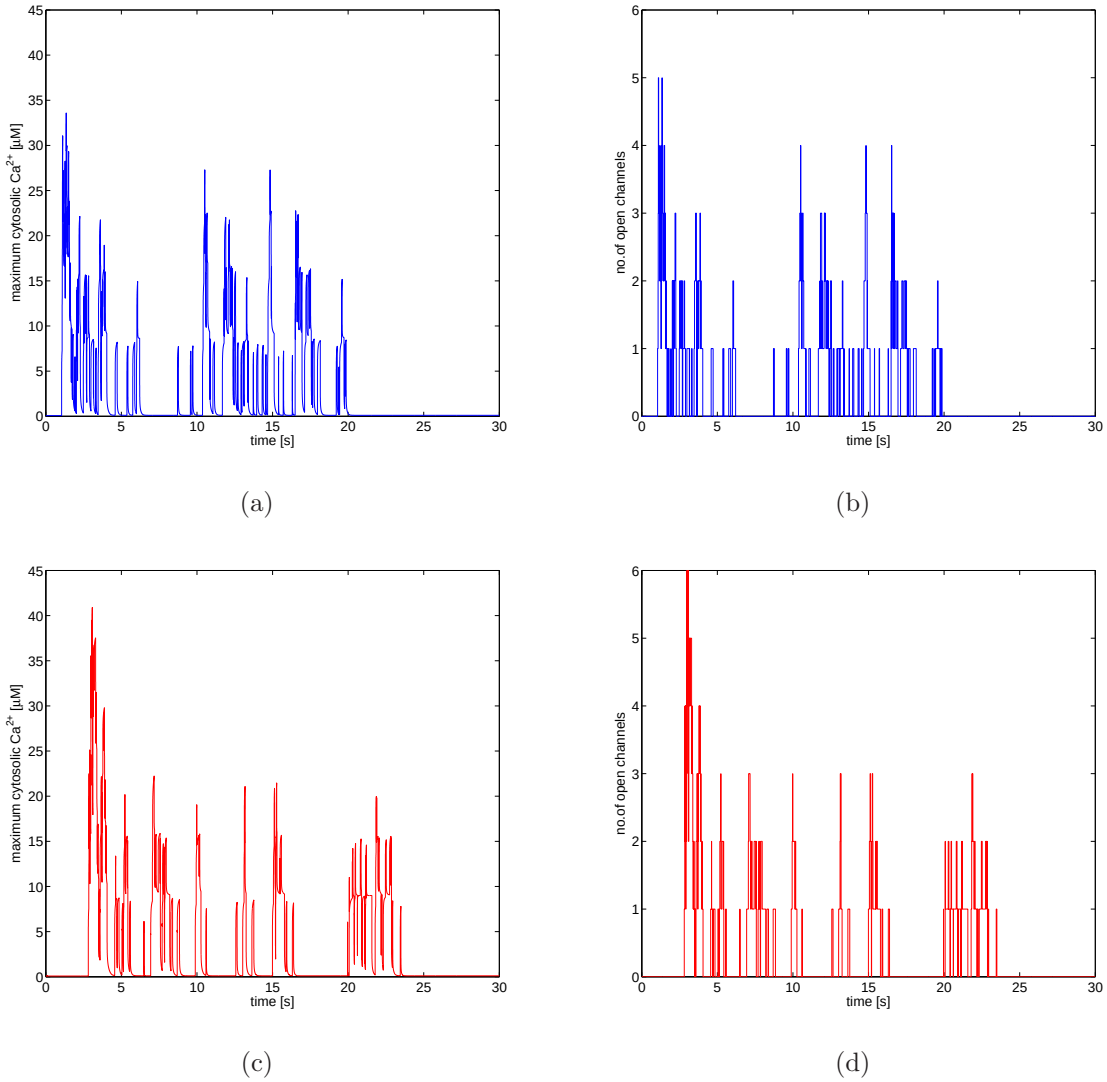

(a) (b)

(c) (d)

Figure 5: Stochastic opening and closing of channels in one cluster arrangement, 5(a)) maximum cytosolic calcium concentration over the simulations time for fixed grid, 5(b)) number of opened/closed channels for fixed grid, 5(c)) maximum cytosolic calcium concentration over the simulation time for adaptive grid and 5(d)) number of opened/closed channels for adaptive grids over the simulation time.

5.2.2 Numerical results with many cluster set up

The numerical results of stochastic opening and closing of channels in an arrangement with 36 clusters are presented in this subsection. The initial coarse grid is shown in Figure 8(a) which is used in the case of adaptive grid refinement, conducted during the intermediate time steps. This mesh consists of 18,792 elements and 9,541 nodal points at mesh level 10.

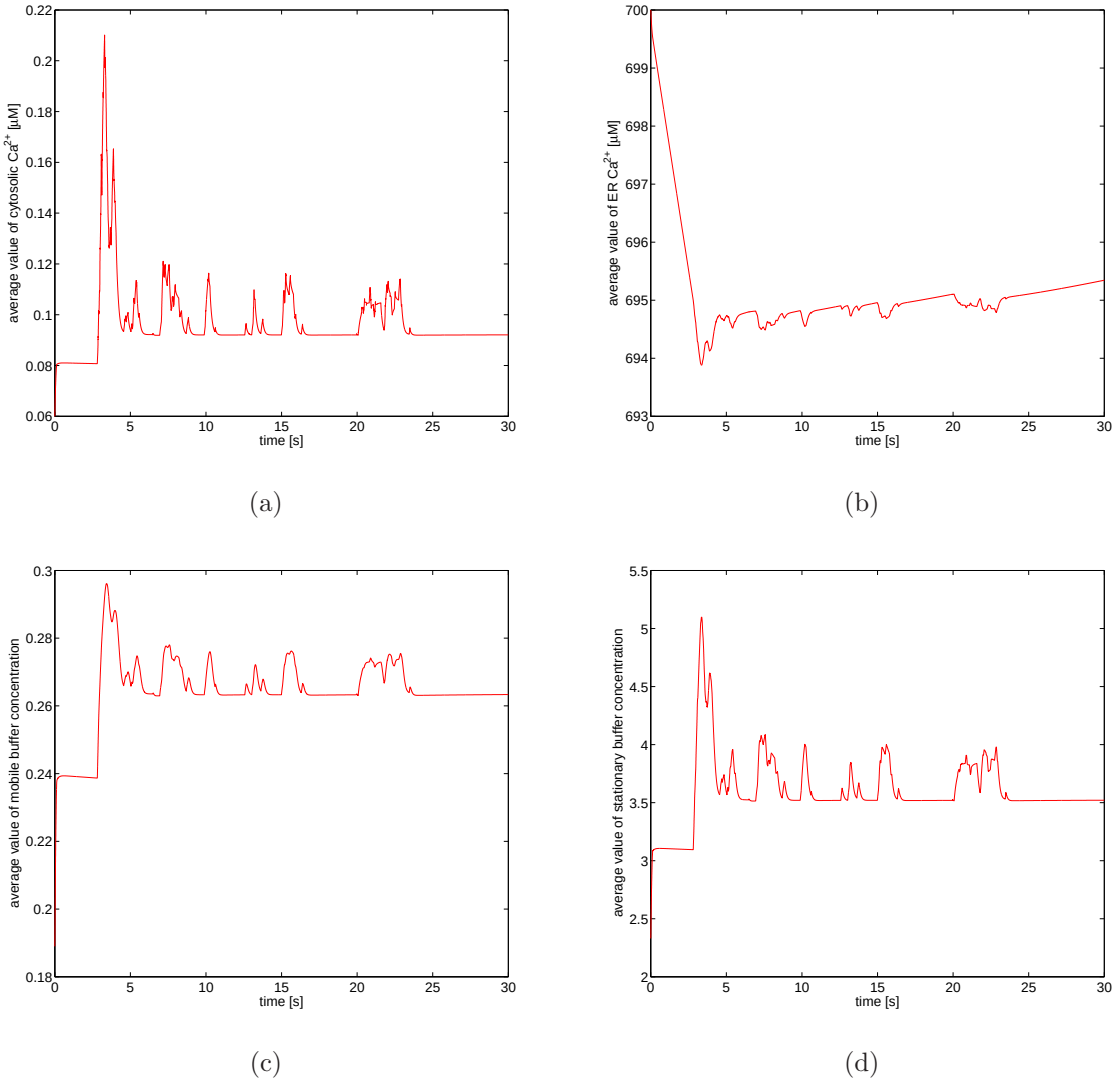

Figure 6: Stochastic Opening and closing of channels in the one cluster arrangement, 6(a)) average value of cytosolic calcium concentration, 6(b)) average value of cytosolic calcium concentration, 6(c)) average value of mobile buffer concentration, 6(d)) average value of stationary buffer concentration for adaptive grids over the simulation time.

The fine (fixed) grid is shown in Figure 8(b) which is used for the other simulations and consists of 62,836 elements and 31,635 nodal points at mesh level 10.

In Figure 9 the maximum cytosolic calcium concentration is plotted for a static grid and a temporal adaptive grid. We can see that with a static grid the maximum Ca^{2+} concentration is about 21.6 µM in Figure 9(a) and the maximum number of open clusters is 30 (Figure 9(c)). In case of a temporal adaptive grid the maximum cytosolic calcium concentration is about 23 µM (see Figure 9(b)) and the maximum number of open clusters

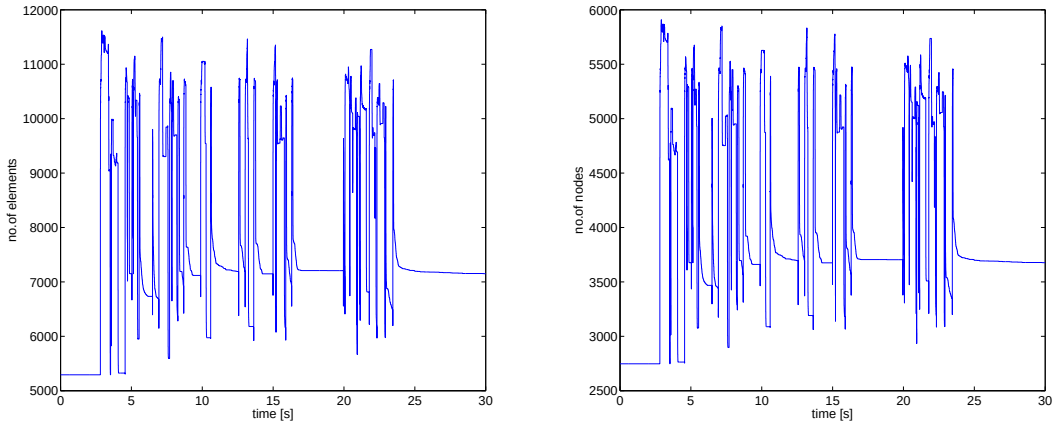

(a) (b)

Figure 7: The evolution of the number of elements in 7(a) and number of points in 7(b) for stochastic channel for 1 cluster arrangement.

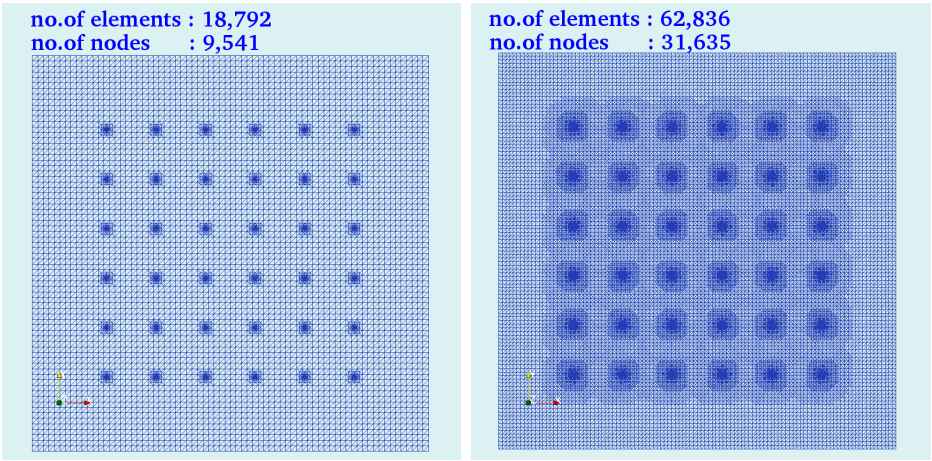

(a) (b)

Figure 8: Different grids considered for the arrangement of the 36 clusters setup 8(a)) coarse grid which is considered as a initial grid for AMR simulations, 8(b)) fixed grid.

is 28 (see Figure9(d)). In this case the difference of Ca^{2+} concentration is at least magnitude of 1.4 μM even though the number of open clusters is less. The corresponding number of open channels for static and temporal adaptive grid is shown in Figure 9(e) and Figure 9(f), respectively. The numbers of refined/coarsened elements and nodal points are depicted in Figure 10. We can see a refinement to about 44,000 elements which consists of 22,000 nodal points when the maximum number of clusters are open. The temporal grid is adjusted

according to opening and closing of clusters and channels in the simulation.

For the comparison of CPU times we found that for the static grid setup the simulation takes 8.897372 days, while for the temporal adaptive grid it takes 6.01 days. For this problem we observed that the temporal adaptive grid performs well over the static grid in terms of an accurate solution as well as computational time.

The contour plots of the solution and the corresponding grid at the different time steps are presented in Figure 11. During this simulation, four clusters are open which consists of 19 open channels at time $t = 0.78262$ s are shown in Figure 11(a) and corresponding grid in Figure 11(b). At this time the grid consists of 38,418 number elements which consists of 19,354 nodes. Likewise, 18 clusters are open which consists of 5 open channels at time $t = 1.75061$ s are shown in Figure 11(c). At time $t = 3.38817$ s, 29 clusters are open which consists of 77 open channels are shown in Figure11(e) and corresponding grid is shown in Figure 11(f).

6 Conclusions

In this article, we have presented an efficient numerical simulation for intracellular calcium dynamics. First we presented numerical results for deterministically opening and closing channels for static and temporal adaptive grids. We have compared several linearly implicit one step methods of Rosenbrock type methods and ROWDA method performed best for this problem. The temporal adaptive numerical solution is accurate as the static grid and more efficient in CPU time as well as in computer memory use. Later, the hybrid numerical solutions are presented for one cluster and 36-cluster arrangements. These numerical results demonstrate that temporal adaptivity is more efficient for higher cluster set ups. We observed that temporal adaptivity is important when channels are opening and closing in the stochastic regime and it is challenging to extend this to higher numbers of clusters in the stochastic regime for three spatial dimensions. Also it is more challenging to find a suitable time stepping method to obtain efficient numerical results in stochastic regime for this type of particular problems. In this case linearly implicit Runge-Kutta methods suit well for this problem. Based on the presented a fully adaptive approach, we are in the process of extending the present implementation to a three dimensional space hybrid model.

Acknowledgements

The authors gratefully acknowledge the Deutsche Forschungsgemeinschaft (DFG), Germany for financial support under the project grants (Fa 350/6-1, Wa 633/16-1). This work was supported in the framework of the DFG priority research program SPP 1095 "Analysis, Modeling, and Simulation of Multiscale Problems".

References

[1] R. A. Adams. *Sobolev Spaces*. Cambridge University Press, 2001.

[2] A. Alfonsi, E. Cancs, G. Turinici, B. Di Ventura, and W. Huisinga. Exact simulation of hybrid stochastic and deterministic models for biochemical systems. *INRIA Rapport de Recherche, Thèmes NUM et BIO*, 5435, 2004.

[3] P. Bastian, M. Blatt, A. Dedner, C. Engwer, R. Klöfkorn, R. Kornhuber, M. Ohlberger, and O. Sander. A generic grid interface for parallel and adaptive scientific computing. Part II: implementation and tests in dune. *Computing*, 82(2):121–138, July 2008.

[4] M. J. Berridge. Calcium oscillations. *J. Biol. Chem.*, 265(17):9583–9586, 1990.

[5] M. J. Berridge. Inositol trisphosphate and calcium signalling. *Nature*, 361:315, 1993.

[6] M. J. Berridge, P. Lipp, and M. D. Bootman. The versatility and universality of calcium signalling. *Nature Rev. Mol. Cell Biol.*, 1:11–22, 2000.

[7] I. Bezprozvanny, J. Watras, and B. E. Ehrlich. Bell-shaped calcium-response curves of $Ins(1,4,5)P_3$- and calcium-gated channels from endoplasmatic reticulum of cerebellum. *Nature*, 351:751–754, 1991.

[8] D. Braess. *Finite elements: Theory, Fast Solvers, and Applications in Solid Mechanics*. Cambridge University Press, 2001.

[9] Elizabeth M. Cherry, Henry S. Greenside, and Craig S. Henriquez. A space-time adaptive method for simulating complex cardiac dynamics. *Phys. Rev. Lett.*, 84(6):1343–1346, Feb 2000.

[10] K. Dekker and J. G. Verwer. *Stability of Runge Kutta methods for stiff nonlinear differential equations*. North Holland Elsevier Science Publishers, 1984.

[11] G. DeYoung and J. Keizer. A single-pool inositol 1,4,5-trisphosphate-receptor-based model for agonist-stimulated oscillations in Ca^{2+} concentration. *Proc. Natl. Acad. Sci. USA*, 89:9895–9899, 1992.

[12] M. Falcke. On the role of stochastic channel behavior in intracellular Ca^{2+} dynamics. *Biophys. J.*, 84(1):42–56, 2003.

[13] M. Falcke. Reading the patterns in living cells - the Physics of Ca^{2+} signaling. *Advances in Physics*, 53(3):255–440, 2004.

[14] M. Falcke, L. Tsimring, and H. Levine. Stochastic spreading of intracellular Ca^{2+} release. *Phys. Rev. E*, 62:2636–2643, 2000.

[15] D. T. Gillespie. Exact stochastic simulating of coupled chemical reactions. *J. Phys. Chem.*, 81:2340–2361, 1977.

[16] K. Gustafsson, M. Lundh, and G. Söderlind. A PI stepsize control for the numerical solution of ordinary differential equations. *BIT*, 28(2):270–287, 1988.

[17] E. Hairer and G. Wanner. *Solving Ordinary Differential Equations II.* Springer Series in Computational Mathematics, 1991.

[18] J. Lang. *Adaptive Multilevel Solution of Nonlinear Parabolic PDE Systems*, volume 16 of *Lecture Notes in Computational Science and Engineering*. Springer-Verlag, Berlin, 2001.

[19] J. Lang and J. Verwer. ROS3P - an accurate third-order Rosenbrock solver designed for parabolic problems. *BIT*, 41(4):730–737, 2001.

[20] J. S. Marchant and I. Parker. Role of elementary Ca^{2+} puffs in generating repetitive Ca^{2+} oscillations. *The EMBO Journal*, 20(1 & 2):65–76, 2001.

[21] R. E. Milner, K. S. Famulski, and M. Michalak. Calcium binding proteins in the sarco/endoplasmatic reticulum of muscle and nonmuscle cells. *Mol. Cell. Biochem.*, 112:1–13, 1992.

[22] Peter K. Moore. An adaptive finite element method for parabolic differential systems: Some algorithmic considerations in solving in three space dimensions. *SIAM Journal on Scientific Computing*, 21(4):1567–1586, 1999.

[23] Ch. Nagaiah. *Adaptive numerical simulation of reaction-diffusion systems.* PhD thesis, Otto-von-Guericke-University Magdeburg, Germany, 2007.

[24] Ch. Nagaiah, S. Rüdiger, G. Warnecke, and M. Falcke. Adaptive numerical solution of intracellular calcium dynamics using domain decomposition methods. *Applied Numerical Mathematics*, 58(11):1658–1674, 2008.

[25] Ch. Nagaiah, S. Rüdiger, G. Warnecke, and M. Falcke. Parallel numerical solution of intracellular calcium dynamics. In U. Langer, M. Discacciati, D.E. Keyes, O.B. Widlund, and W. Zulehner, editors, *Domain Decomposition Methods in Science and Engineering XVII*, volume 60 of *Lecture Notes in Computational Science and Engineering*, pages 155–164, Heidelberg, 2008.

[26] J. W. Putney and G. S. J. Bird. The inositolphosphate-calcium signaling system in nonexcitable cells. *Endocrine Reviews*, 14(5):610–631, 1993.

[27] A. Quarteroni and A. Valli. *Numerical Approximation of Partial Differential Equations.* Springer Series in Computational Mathematics, 1994.

[28] E. B. Ridgway, J. C. Gilkey, and L. F. Jaffe. Free calcium increases explosively in activating medaka eggs. *Proc. Natl. Acad. Sci. USA*, 74:623–627, 1977.

[29] T. A. Rooney, E. J. Sass, and A. P. Thomas. Characterization of cytosolic calcium oscillations induced by phenylephrine and vasopressin in single fura-2-loaded hepatocytes. *J. Biol. Chem.*, 264:17131–17141, 1989.

[30] S. Rüdiger, J. W. Shuai, W. Huisinga, Ch. Nagaiah, G. Warnecke, I. Parker, and M. Falcke. Hybrid stochastic and deterministic simulations of calcium blips. *Biophys. J.*, 93:1847–1857, 2007.

[31] B. A. Schmitt and R. Weiner. Matrix-free W-methods using a multiple Arnoldi iteration. *Appl. Num. Math.*, 18:307–320, 1995.

[32] J. Smoller. *Shock Waves and Reaction-Diffusion Equations.* Springer-Verlag, New York, 1995.

[33] Vidar Thomée. *Galerkin Finite Element Methods for Parabolic Problems (Springer Series in Computational Mathematics).* Springer-Verlag New York, Inc., Secaucus, NJ, USA, 2006.

[34] John A. Trangenstein and Chisup Kim. Operator splitting and adaptive mesh refinement for the Luo-Rudy I model. *J. Comput. Phys.*, 196(2):645–679, 2004.

[35] R. Verfürth. A review of a posteriori error estimation and adaptive mesh-refinement techniques. *Wiley & Teubner*, 1996.

[36] Z. Zhou and E. Neher. Mobile and immobile calcium buffers in bovine adrenal chromaffin cells. *J. Physiol.*, 469:245–273, 1993.

[37] O. C. Zienkiewicz and J. Z. Zhu. A simple error estimator and adaptive procedure for practical engineering analysis. *Int. J. Num. Meth. Eng*, 24:337–357, 1987.

Parameter	Value	Unit
leak flux coefficient P_l	0.025	s^{-1}
channel flux coefficient P_{ch}	3.0×10^3	$\mu m\ s^{-1}$
single channel radius R_s	0.018	μM
pump flux coefficient P_p	100	$\mu m\ \mu M\ s^{-1}$
pump dissociation coefficient K_d	0.04	μM
diffusion coefficient D of free cytosolic Ca^{2+}	200	$\mu m^2\ s^{-1}$
diffusion coefficient D of free ER Ca^{2+}	200	$\mu m^2\ s^{-1}$
diffusion coefficient D_m of mobile buffer	40	$\mu m^2\ s^{-1}$
diffusion coefficient D_s of stationary buffer	0.01	$\mu m^2\ s^{-1}$
on-rates of fast buffers:		
k_s^+	200	$(\mu M\ s)^{-1}$
k_m^+	400	$(\mu M\ s)^{-1}$
dissociation constants of buffers $K_i = \frac{k_i^-}{k_i^+}$:		
K_s	2	μM
K_m	0.25	μM
total concentrations of buffers:		
B_s	80	μM
B_m	1	μM
subunit kinetics, note $b_i=a_i d_i$, i=1,...,5		
IP3 binding		
a_1, a_3	20	$(\mu M\ s)^{-1}$
d_1	0.13	μM
d_3	0.13	μM
inhibiting, with IP3		
a_2	0.030373	$(\mu M\ s)^{-1}$
d_2	3.776	μM
inhibiting, without IP3		
a_4	0.303073	$(\mu M\ s)^{-1}$
d_4	0.5202	μM
activating		
a_5	2.222	$(\mu M\ s)^{-1}$
d_5	0.3	μM

Table 2: Parameters used in the numerical simulations.

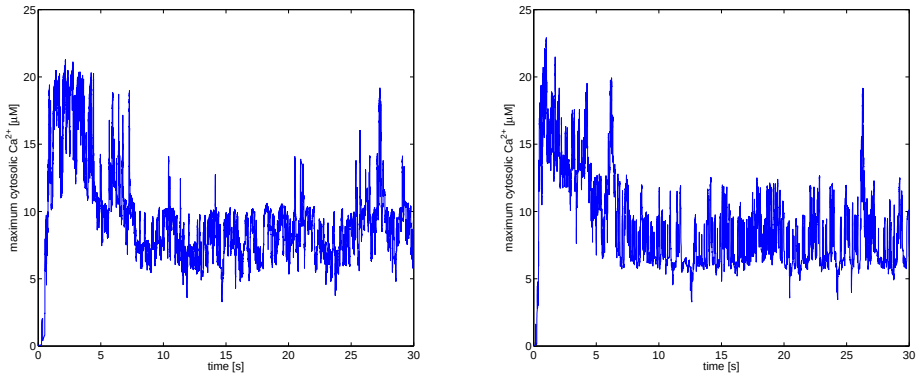

(a)

(b)

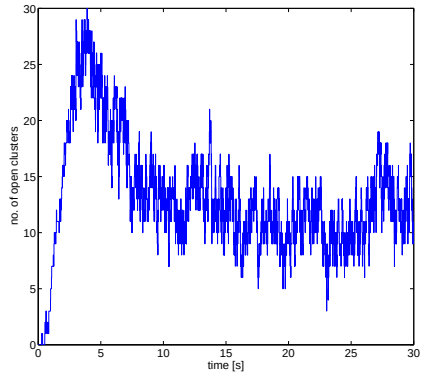

(c)

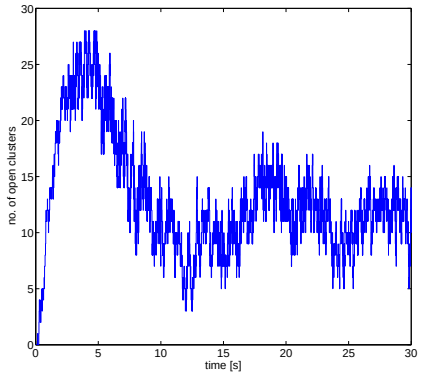

(d)

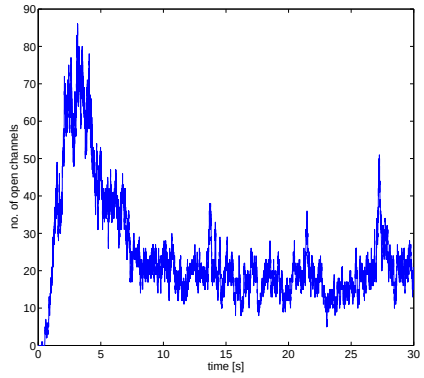

(e)

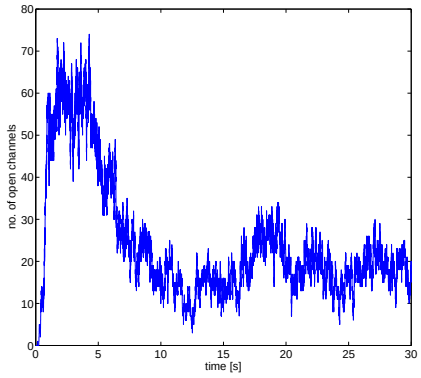

(f)

Figure 9: Stochastic Opening and closing of channels in the 36 clusters arrangement, maximum cytosolic calcium concentration over the simulations time for fixed grid in 9(a)) and for temporal adaptive grid in 9(b)), number of opened/closed clusters for fixed grid in 9(c) and for temporal adaptive grid in 9(d), number of opened/closed channels for fixed grid in 9(e) and for temporal adaptive grid in 9(f), over the simulation time.

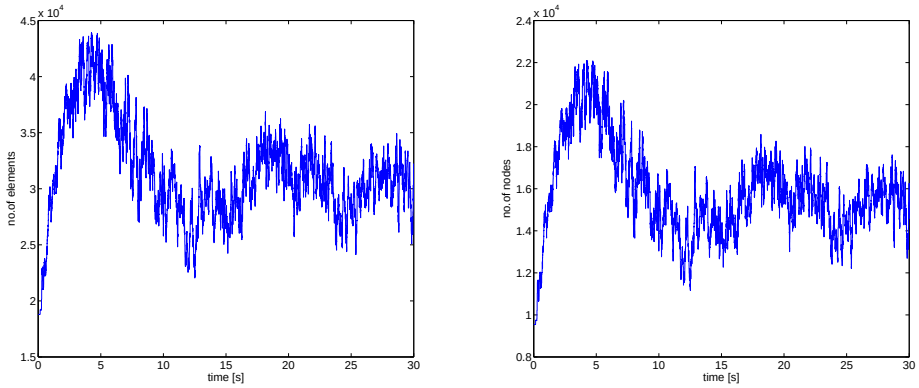

Figure 10: Stochastic Opening and closing of channels in the 36 clusters arrangement for temporal adaptive grid, the number of refined/coarsened elements at left and nodal points at right.

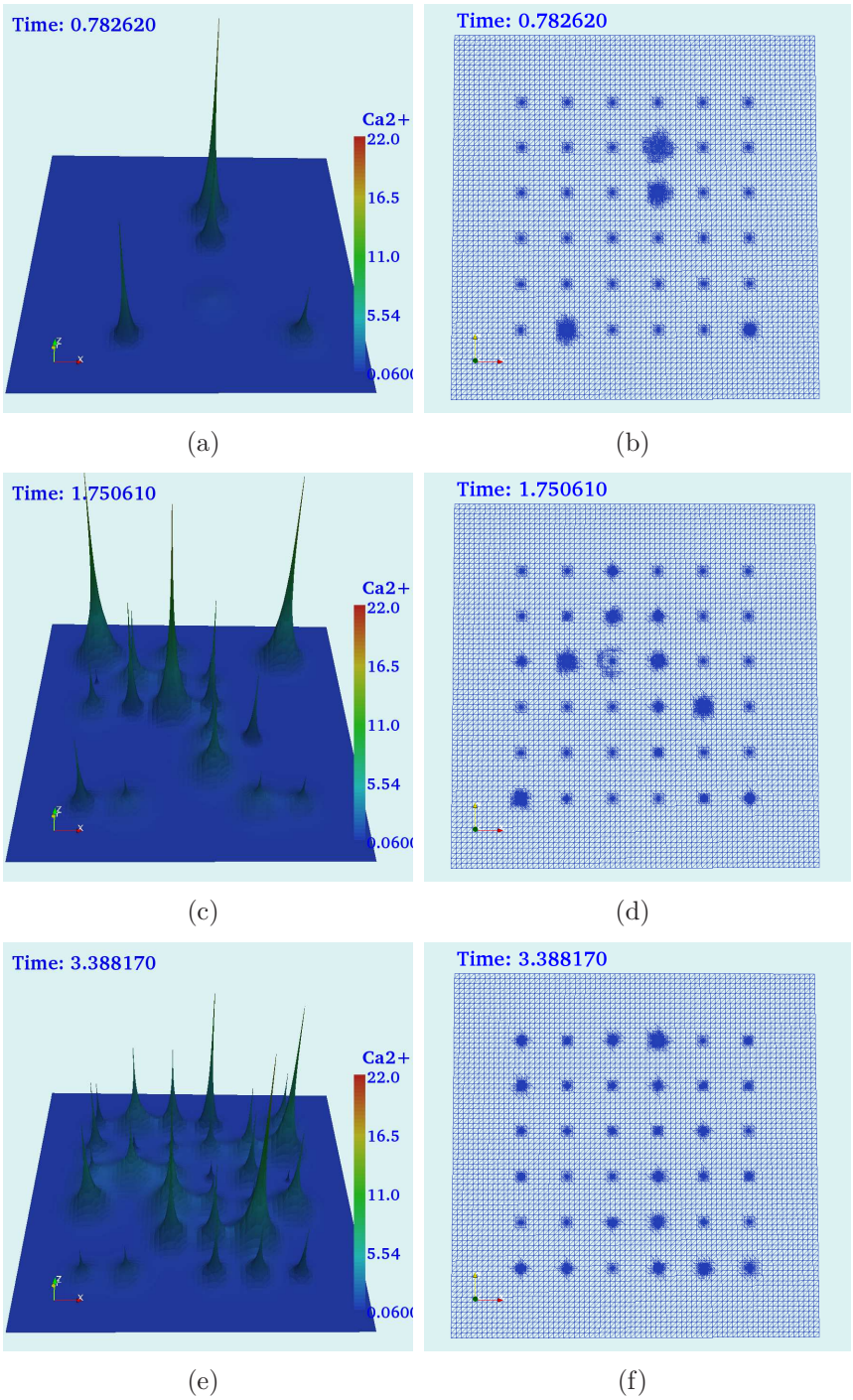

Figure 11: The contour and grid plots of the stochastic channel transition for the 36 clusters arrangement, the contour plot of the cytosolic Ca^{2+} at time $t = 0.78262$ s in 11(a)) and corresponding grid in 11(b)), the contour plot of the cytosolic Ca^{2+} at time $t = 1.75061$ s in 11(c)) and corresponding grid in 11(d)), the contour plot of the cytosolic Ca^{2+} at time $t = 3.38817$ s in 11(e)) and corresponding grid in 11(f)).